Extended Abstract for the 40th Aerospace Sciences Meeting & Exhibit
To be held in Reno, NV, January 14-17, 2002

Parametric Time-Dependent Navier-Stokes Computations for a YAV-8B Harrier in Ground Effect

Neal M. Chaderjian* and Shishir Pandya,†
NASA Ames Research Center, Moffett Field, California 94035
and
Jasim Ahmad‡ and Scott Murman§
ELORET, Moffett Field, California 94035

Introduction

The Harrier Jump Jet has the distinction of being the only powered-lift aircraft in the free world to achieve operational status and to have flown in combat.[1] This V/STOL aircraft can take-off and land vertically or utilize very short runways by directing its four exhaust nozzles towards the ground. Transition to forward flight is achieved by rotating these nozzles into a horizontal position. Powered-lift vehicles have certain advantages over conventional strike fighters. Their V/STOL capabilities allow for safer carrier operations, smaller carrier size, and quick reaction time for troop support. Moreover, they are not dependent on vulnerable land-based runways. The AV-8A Harrier first entered service in the British Royal Air Force (RAF) during 1969, and the U.S. Marine Corps (USMC) in 1971. The AV-8B was a redesign to achieve improved payload capacity, range, and accuracy. This modified design first entered service with the USMC and RAF in 1985. The success and unique capabilities of the Harrier has prompted the design of a powered-lift version of the Joint Strike Fighter (JSF).

The flowfield for the Harrier near the ground during low-speed or hover flight operations is very complex and time-dependent. A sketch of this flowfield is shown in Fig. 1. Warm air from the fan is exhausted from the front nozzles, while a hot air/fuel mixture from the engine is exhausted from the rear nozzles. These jets strike the ground and move out radially forming a ground jet-flow. The ambient freestream, due to low-speed forward flight or a headwind during hover, opposes the jet-flow. This interaction causes the flow to separate and form a ground vortex. The multiple jets also interact with each other near the ground and form an upwash or jet fountain, which strikes the underside of the fuselage. If the aircraft is sufficiently close to the ground, the inlet can ingest ground debris and hot gasses from the fountain and ground vortex. This Hot Gas Ingestion (HGI) can cause a sudden loss of thrust (powered lift), and the vehicle may crash. The high-speed jet flow along the ground can also entrain the ambient flow, resulting in a low pressure region underneath the vehicle. The accompanied loss of lift is referred to as the suckdown effect. The ground vortex may also be highly unsteady, dramatically changing its size and position with time at low frequencies, e.g., 1 Hz.[2]

---

[*] Research Scientist, Associate Fellow AIAA.

[†] Research Scientist, Member AIAA.

[‡] Senior Research Scientist.

[§] Senior Research Scientist, Member AIAA.

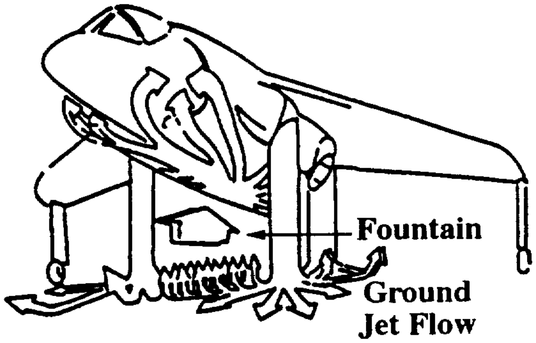

Fig. 1 Harrier flowfield in ground effect

A number of numerical and experimental investigations have been carried out to better understand the complex time-dependent flows associated with powered-lift vehicles. One approach is to vastly simplify the geometry to study the basic flow physics. Following this approach, Van Daisem et.al.[3] numerically simulated the flow for an isolated round jet in crossflow using the time-dependent Reynolds-averaged Navier-Stokes (RANS) equations. The jet and ground vortex were found to be steady when the freestream to jet velocity ratio was $V_\infty/V_{jet}=0.223$, and the height ratio was $h/D_{jet}=3$. Some unsteadiness was found, however, when the velocity ratio was lowered to $V_\infty/V_{jet}=0.1$. The location of the ground vortex was found to be a strong function of the turbulent mixing in the ground-vortex region. Modifications were made to the Baldwin-Lomax turbulence model[4] so that the ground-vortex position was in better agreement with experiment. Vortex rings were found to shed from the jet when it was impulsively pulsed. The unsteady flow was found to damp to the original steady result. Jets in crossflow with elliptic cross were also computed.

A follow-on work by Van Dalsem et.al.[5] included the effects of ground-plane heating and a RANS simulation using a delta wing in ground effect with two aft mounted thrust-reverser jets. The delta wing computations captured the loss of lift associated with the suckdown effect and the small drop-off of lift at higher positions above the ground plane due to the conventional ground cushion effect. Preliminary results were also presented for a Harrier YAV-8B forebody and inlet.

Barata et.al.[6] carried out RANS simulations for an isolated round jet in crossflow, and an extension of this work by Barata[7] included multiple jets in crossflow. The jet velocities and heights above the ground plane were similar to the previously cited references. This work focused on the validation of a new numerical method using the k-ε turbulence model.[8] The overall flow features were captured and compared to experiment. Prediction of the velocity, Reynolds shear-stress, and ground-plane surface pressures were adequate.

Additional geometric complexity has been numerically investigated by introducing delta wings with jets in the presence of a ground plane. Chawla and Van Dalsem[9] carried out time-accurate laminar RANS solutions for a delta wing with two aft mounted thrust-reverser jets, the same geometry described in Ref. 5. These jets were pointed downward with a forward inclination of 45 degrees. Static flow simulations were computed at span heights ranging from 0.25 to 1.0 above the ground plane. A flow simulation with the delta wing descending towards the ground plane was also presented. The static cases showed the proper trends between the lift coefficient (C_L) and height, including the suckdown and cushion effects. The flows were found to be very unsteady, with Strouhal numbers ($St=fD_{jet}/V_\infty$) ranging from 0.015 to 0.03. Chawla and Van Dalsem make the point that certain approximations had to be made in order to reduce the very long compute times to more manageable levels.

Roth[10] also carried out RANS flow simulations about a simplified powered-lift geometry, which consisted of a cropped delta wing with a blended fuselage and two circular jets mounted in tandem on the underside of the wing. Both laminar and turbulent computations were compared with each other and experimental data. The Balwin-Lomax turbulence model with the Degani-Schiff[11] modification for vortices was utilized for turbulent computations. Comparisons of computed flows with experiment showed fair agreement. Neither the laminar or turbulent computations completely characterized the wing leading-edge and near jet flow fields. Qualitative features, such as jet-induced lift loss (suckdown) were captured. Again, the point was made for the need of faster solution methods.

There have been very few RANS computations for the Harrier reported in the literature. Gea et.al.[12] computed steady transonic flow about the Harrier YAV-8B wing with pylons. This work focused on the shock-induced separation near the wing/pylon juncture. Better turbulence models and faster solutions methods were again an issue. Mysko et.al.[13] simulated steady transonic flow for a Harrier forebody/inlet geometry using the RANS equations. Many of the global trends were captured, including surface pressures at the cowl lip, fuselage/inlet wall, and engine face region.

Smith et.al.[14] presented a RANS solution about a simplified YAV-8B Harrier in ground effect. The aircraft was 30 feet above the ground plane, with a freestream Mach number of 0.04 (30 Knots) and an angle of attack of 8 degrees. The Harrier geometry included a fuselage, wing, leading edge root extension (LERX), inlets, and the exhaust nozzles. The empennage, deflected flap, and lift-improvement devices (LID) on the underside of the fuselage were not modeled. To date, this represents the only RANS solution about a fairly complete Harrier aircraft in ground effect. The OVERFLOW[15] computational fluid dynamics (CFD) code was used, together with its overset grid capability for treating complex geometries. Again, a strong point was made for faster solution methods. In order to offset the long compute times, certain simplifications were made to the time-accurate approach. Local time stepping was used in viscous regions near the body, and a constant time step was used outside the boundary layer. This allowed for a more efficient flow simulation. Smith felt that this approach would still capture the unsteady features in the flow.

The references cited above indicate two important obstacles remain in simulating powered-lift flows in ground effect using the time-accurate RANS equations. There is a need for improved accuracy, and there is a need for faster solution methods. We view the latter as key to enabling the assessment and improvement of solution accuracy. The purpose of this paper is to describe a process that has enabled 45 time-accurate RANS solutions about a YAV-8B Harrier aircraft in ground effect. The eventual goal is to compute enough solutions to define a stability and control (S&C) database. Ultimately, it is envisioned that a few hundred solutions can be obtained, and the remainder of the parameter space "filled out" with the use of neural networks. This paper is a first step towards that goal.

The next section describes the solution procedure. This includes a description of the parameter space used in this study, the automated grid generation and solution process, turbulence model, and boundary conditions. This is followed by a discussion of results and concluding remarks.

Solution Procedure

Aerodynamic Coefficients

The lift coefficient (C_L) is assumed to take the form of Eq. (1). The primary independent

$$C_L = C_L(\alpha , h , V , T , \delta_{control} , \frac{d\alpha}{dt} , q , \ldots) \tag{1}$$

variables are: angle of attack (α), vehicle height above the ground plane (h), freestream velocity (V), thrust setting (T), control surface deflections ($\delta_{control}$), time derivative of angle of attack ($\frac{d\alpha}{dt}$), and pitch rate (q). An aerodynamic model for the lift coefficient can be established in the usual manner using the static and dynamic stability derivatives. The first 5 variables define the static terms while the last two define the dynamic portion of the model. For the present study, we are only allowing the angle of attack and height to vary. The angle of attack varies from 4-12 degrees, with 1 degree increments. The height of the aircraft center of gravity above the ground plane varies from 10-30 feet, with 5 foot increments. Thus a total of 45 static cases are computed. All other parameters are fixed in order to keep the parameter space to a manageable level. The number of independent parameters can be increased at another time. The drag and pitching moment coefficients have similar forms to the lift coefficient.

Grid Generation

An overset grid system was developed using Chimera Grid Tools[16]. The overset surface grids of Smith et.al[14] were used as a starting point to define the Harrier geometry. A completely new overset surface grid system was then developed to improve the grid quality and interzone connectivity. The empennage and deflected flap were also included from lofting line data originally obtained from the airframe manufacturer. Figure 2 show front and rear views of the new overset surface grid system. Volume grids were then generated, with viscous clustering near the body such that y^+ never exceeded 5 at the first grid point off the body. The Harrier volume grid system was then imbedded into a Cartesian box grid. This "aircraft" box grid connects the Harrier volume grids to the ground plane and far-field grids.

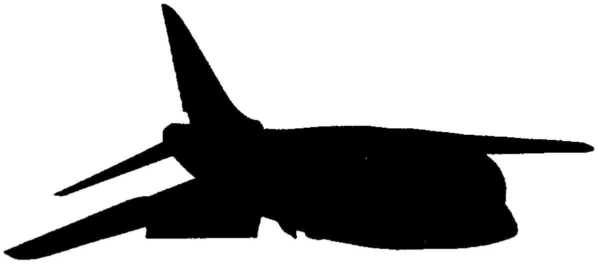

Fig. 2a Front view of surface grids.

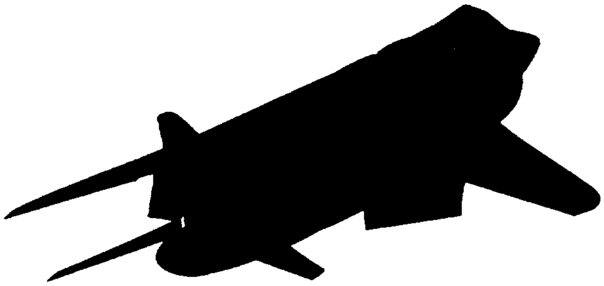

Fig. 2b Rear view of surface grids.

The ground plane and jet grids are shown in Fig. 3. Notice that the angle of attack and vehicle height above the ground plane are built into the grid system. It was necessary to include fine-spaced jet grids to accurately resolve the jet-flow between the exhaust nozzles and the jet/ground-plane impact region. In fact, when the Harrier is 30 feet above the ground plane, these two jet grids comprise 1/3 of the grid points for the entire grid system. Viscous spacing was used at the ground-plane to accurately resolve the ground jet flows and ground vortex. Additional Cartesian box grids connect the aircraft box grid, jet grids, and the ground plane to the far field.

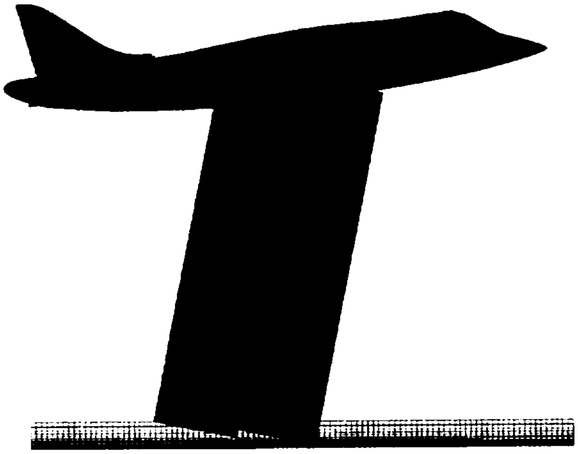

Fig. 3 Side view of jet and ground plane grids.

An object-oriented PERL script system was developed to automatically generate the grid systems for all 45 cases. This process begins by developing the above grid system in the usual manual manner for a specific height and angle of attack. The zonal grid topology is designed so that this base grid system can be used to generate all of the grid systems with simple translations and rotations. Any portion of the jet grids that extend below the ground plane are removed, thus improving computational efficiency. The viscous grid spacing near body and wall boundaries can also be specified in the PERL script. This grid generation process is fairly robust because the intergrid connection between the Harrier grids and the aircraft box grid remains fixed. The grid connectivity only changes between this aircraft box grid and all other exterior grids. The entire grid generation process, including the intergrid communication through the Pegasus 4.1 code,[17] are all controlled in an automated manner with the PERL script. The half-body grid system used in the present flow simulations consists of 52 zones and 3.1-3.6 million grid points, depending on the height of the aircraft above the ground plane. Additional detail for the entire grid generation process can be found in Murman et.al.[18]

Numerical Algorithm

The time-dependent Reynolds-averaged Navier-Stokes equations are numerically solved using overset body-conforming structured grids and the OVERFLOW-MLP code. The implicit Pulliam-Chausse[19] diagonal central-difference algorithm is used for the present computations. Blended 2nd and 4th-order numerical dissipation is added to damp high-frequency errors. The method is first-order accurate in time and second-order accurate in space. Time accuracy for viscous computations are normally limited by algorithm stability rather than accuracy requirements. It will be shown in the Results section that this is the case for the present set of computations. The thin-layer approximation is used on all grids attached to solid surfaces. The full Navier-Stokes equations, including explicit cross terms, are used in the jet-exhaust grids. The Euler equations are used on all of the remaining grids. These grids are typically the far-field box grids.

The normal production version of OVERFLOW[15] utilizes loop-level parallelism. This approach when applied to implicit algorithms, which are typically required for viscous flow computations, encounter a rapid loss of parallel efficiency as more processors are utilized. Typically 4-8 processors are the maximum one uses. Taft[20] introduced domain decomposition into the OVERFLOW code as a way to improve its parallel efficiency. Domain decomposition essentially groups together several zones and assigns several processors to each group. This allows for improved parallel performance and scalability. The OVERFLOW-MLP code used in this study uses this multi-level parallel (MLP) approach, i.e., loop-level parallelization and domain decomposition. The user simply chooses the number of groups and processors to obtain the best acceptable performance. The domain decomposition algorithm in the code decides how many processors to allocate to each group. It seeks to allocate the same number of grid points to each group. However, weights can be adjusted to account for the difference in work associated with the Euler, thin-layer, and full Navier-Stokes fidelities. The rest of the input variables are identical to the original OVERFLOW code.

Turbulence Model

As the introduction indicates, modeling the turbulence for powered-lift flows can be a challenge. Some have used the Baldwin-Lomax algebraic (zero equation) model primarily for its computational efficiency, and modified it to improve its accuracy. Others have gone to the more costly two equations models, e.g., the k-ε model. Both models do a reasonable job in modeling the qualitative features of the flow. They also do an adequate job of quantifying the turbulence effects. Neither seems to work universally well. So a compromise is adopted here. The one-equation Spalart-Allmaras[21] turbulence model is used for all of the computations presented in this paper. This model is more efficient than the two-equation models and probably as accurate. It also provides a more satisfactory modeling of turbulent flow than the algebraic models.

Boundary Conditions

The boundary conditions used in this parameter study follow those used by Smith et.al.[14] The freestream Mach number, however, is set to 0.05 (33 kts) rather than 0.04 in Ref. 14. The angle of attack varies from 4-12 degrees with a one degree increment, and the height varies from 10-30 feet with a five foot increment. The Reynolds number, based on the body length is Re=15.2 million. Standard sea-level conditions are assumed.

All solid surfaces on the aircraft employ the no-slip condition. The viscous ground plane, however, is treated differently. The actual vehicle moves over the stationary ground with a zero ambient freestream. A simple transformation is employed so that none of the grids need to move. The aircraft is treated as stationary, and the freestream velocity is imposed at all far-field boundaries, and on the ground plane. This simulates the aircraft moving forward into a stationary flow. The pressure and density on all solid surfaces are obtained by extrapolation. Outflow variables are obtained at the downwind far-field boundary using simple upwind extrapolation.

Inlet grids continue internally up to the compressor face where an average pressure is imposed to control the mass flow. The pressure distortion just upstream of the compressor is added to this mean pressure. The remaining flow variables are obtained by extrapolation. Thus flow distortion is allowed at the compressor face. Since thrust remains constant for this set of parametric computations, the same inlet and nozzle flow conditions are imposed for all cases. The mass flow used in these computations is identical to the one Smith[14] obtained from an engine-deck analysis.

The front and rear nozzle velocities and temperatures are specified according to Table 1. The remaining flow variables are obtained by extrapolation. These nozzle conditions correspond to the "short-lift wet" engine thrust setting.

	Front Nozzle Conditions	Rear Nozzle Conditions
M	0.7883	0.7644
V	1003 ft/s	1489 ft/s
Temp	672.9 °*R*	1578.2 °*R*

Table 1 Specified nozzle boundary conditions.

Solution Automation

Automation is an important element in managing a parametric RANS analysis. For example, the present study produced more than a terabyte of data and thousands of files. This data resides on a Unix-based mass storage system. The PERL scripts used for storage and retrieval of data map the flow parameters into a Unix directory structure. The user simply specifies the flow parameters, e.g., h=30, $\alpha=9^\circ$, and the scripts take care of the rest. The grid-generation scripts described earlier automatically generate all of the necessary grids, run them through the Pegasus code, and store all of the files needed to run the OVERFLOW-MLP code onto the mass storage system. Another script system runs the flow solver. The flow-simulation script automatically fetches data for the mainframe, a 512 processor 400MHz/R12000 Silicon Graphics Origin 2000 single-image machine, and executes the OVERFLOW-MLP code. Once a job is complete, the output files are automatically stored on the mass storage system. A unique run-number is appended to the stored files. If more runs are needed, the script resubmits itself on the mainframe. A typical flow simulation consisted of running 9 cases concurrently, i.e., all 9 angles of attack for a given height. Sixteen processors were assigned to each case, for a total of 144 processors. Any number of cases can be run concurrently, and in any order, depending on the number of available processors. This 9 case example using 144 processors required about 125,000 time steps and 28,000 CPU-hours, or 8 days of continuous computation on an SGI O2K machine. The nondimensional time step, $\Delta\tau=0.002$, is typical of time-accurate RANS solutions about complete aircraft geometries. The long run times were required to resolve very low dominant frequencies with periods on the order of 2 seconds of physical time. Typically, three periods of oscillation were used to compute mean forces and moments. The source of these long-period oscillations is described in the Results section.

A PERL GUI (DBVIEW) was developed to simplify the post-processing of data. One can select any number of cases from the database, and the results will be graphically displayed or sent to a printer. Graphically displayed data can take the form of 2D plots or 3D flow visualization. Further details describing the script systems and automation can be found in Ref. 18.

Results

Fortyfive time-dependent RANS flow simulations have been computed, where the angle of attack range was $4^\circ \le \alpha \le 12^\circ$, and the height range was $10\text{ft} \le h \le 30\text{ft}$. The Mach number was fixed at M=0.05 (33kts), and the Reynolds number based on the body length was Re=15.2 million. Due to the danger of HGI and the suckdown effect, a Harrier pilot will not ordinarily maintain a constant altitude of less than 30 feet when operating at very low speeds or hover flight conditions. However, typical aerodynamic models require the static stability derivatives, or forces and moments, near the ground to simulate take-off and landing scenarios. Therefore static computations have been carried out in this height range.

Most of the cases were found to be highly unsteady. A constant nondimensional timestep of $\Delta\tau=0.002$ was used for all 45 cases, and throughout the entire flow domain. This corresponds to a physical time step of 76.6 μs. This was the largest allowable time step that maintained algorithm stability for the entire parameter range. Figure 4 shows how the time step affects the temporal aerodynamic lift coefficient for one of the more unsteady cases. The time step was reduced by factors of 2 and 4. Reducing the time step by a factor of 2 only slightly affected the lift time history. The mean values of lift differed only by 0.3%. Reducing the time step further by a factor of 4 had virtually no effect. The frequency content was not significantly affected by the time step refinement. The largest time step provided about 26,000 time steps per cycle for the dominant aerodynamic frequencies, and about 3,000 time steps per cycle for the higher frequencies. Overall, the largest stable time step ($\Delta\tau=0.002$) did a good job of resolving the temporal features of the flow with the least computational cost, and was therefore used for all the computations in this paper.

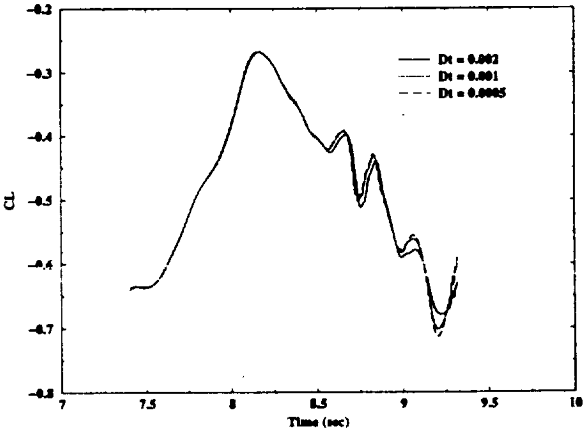

Fig. 4 Effect of time-step on lift coefficient for h=30ft, $\alpha=9^\circ$ and V=33kts.

(A grid refinement study where the body resolution will be increased by a factor of two on the wing and horizontal tail will be presented in the final paper.)

Figure 5 shows an automated composite flow visualization image obtained from DBVIEW. The top two images show instantaneous streamlines colored by temperature. The horseshoe ground vortex is clearly visible, as are the fountain effects. Notice that jet-fountain streamlines strike the underside of the fuselage. This is particularly apparent on the aft portion of the fuselage. A secondary vortex also forms in front of the primary ground vortex. A jet fountain near the flow symmetry plane is able to traverse the ground vortex and move upstream of it. This flow then forms a vortex due to the close proximity of the engine inlets and is drawn into the inlet. As expected, HGI is a problem at this height. The lower-right quadrant of Fig. 5 shows a top view of the instantaneous surface-flow patterns on the ground plane. The Harrier is rendered semi-transparent to allow viewing of the ground plane, which is colored by temperature. The separation line caused by the formation of the ground vortex, and the locations where the jets impact the ground are also visible. The lower-left quadrant shows the temperature variation on the underside of the fuselage. The aft portion of the fuselage is particularly hot due to the jet fountains. Automated composite figures, such as the one shown in Fig. 5, provide a quick qualitative assessment of the dominant flow features in a large parameter study.

Fig. 5 Automated composite flow visualization for the Harrier in ground effect. Blue/red colors correspond to cool/hot temperatures. M=0.05 (33 kts), h=30ft, $\alpha=9^{\circ}$.

All cases were run in the same manner. The solution process begins by running 300 multigrid steps from an impulsive start condition. A constant time step is then used for the remainder of the computation. The initial use of multigrid helps establish the flow and provides improved robustness to the startup process. Different startup strategies were investigated, including running multigrid for longer periods of time, and the use of local time steps as a means to transition to a constant time step. All of these strategies prolonged the transient portion of the flow simulation. The overuse of multigrid, or using local time steps, introduces spurious unsteady modes (transients) that persist for long periods of times. The best strategy seems to be to use multigrid for a short time to help the solution get started, then switch to a constant time step as soon as possible.

The lift coefficient time history and power spectra is shown in Fig. 6 for M=0.05 (33 kts), h=30ft and $\alpha=9^\circ$. This particular case is representative of the solution database. It can be seen that the lift time history is not purely periodic. This is not surprising due to the complexity of the flow. The power spectra (FFT) indicates a fundamental (lowest) frequency of f=0.478 Hz. The computed mean aerodynamic lift coefficient is $\overline{C_L}=-0.480$, with a standard deviation of 0.157. The aerodynamic lift coefficient is negative. Smith et.al.[14] reported an even larger negative lift in their RANS solution because their geometry did not include a deflected wing flap and empennage. It is difficult to achieve positive aerodynamic lift near the ground due to the suckdown effect. This is why the AV-8B also has lift improvement devices (LIDS) on the underside of the vehicle. The LIDS were not included in the present computations. Engine thrust provides the needed lift to support the vehicle in hover. Flow visualization indicates that even at positive angles of attack, the high-speed jet flow strongly entrains the low-speed freestream, resulting in an effective negative angle of attack near the wing leading edge. Cimbala et.al.[2] also measured frequencies as low as 1 Hz for a round jet in crossflow. This experimental value had a velocity ratio of $V_\infty/V_{jet}=0.05$, the same as the front Harrier jets. This frequency corresponds to a Strouhal number $St=f\,D_{jet}/V_\infty=0.017$. The Strouhal number for the Harrier, based on the equivalent diameter of the front jets, is St=0.011. It is recognized that the experiment of Cimbala is for a single round jet in crossflow, which is much closer to the ground than the Harrier jets. Moreover, the Harrier is a more complex geometry with multiple jets that have near rectangular cross-sections. However, the similarities of the low frequencies (and Strouhal numbers) is encouraging. Unfortunately there is a lack of experimental data for a Harrier in ground effect that is suitable for detailed CFD validation.

(A comparison of the computed jet trajectories with those observed in an infrared flight-test photograph will also be included in the final paper.)

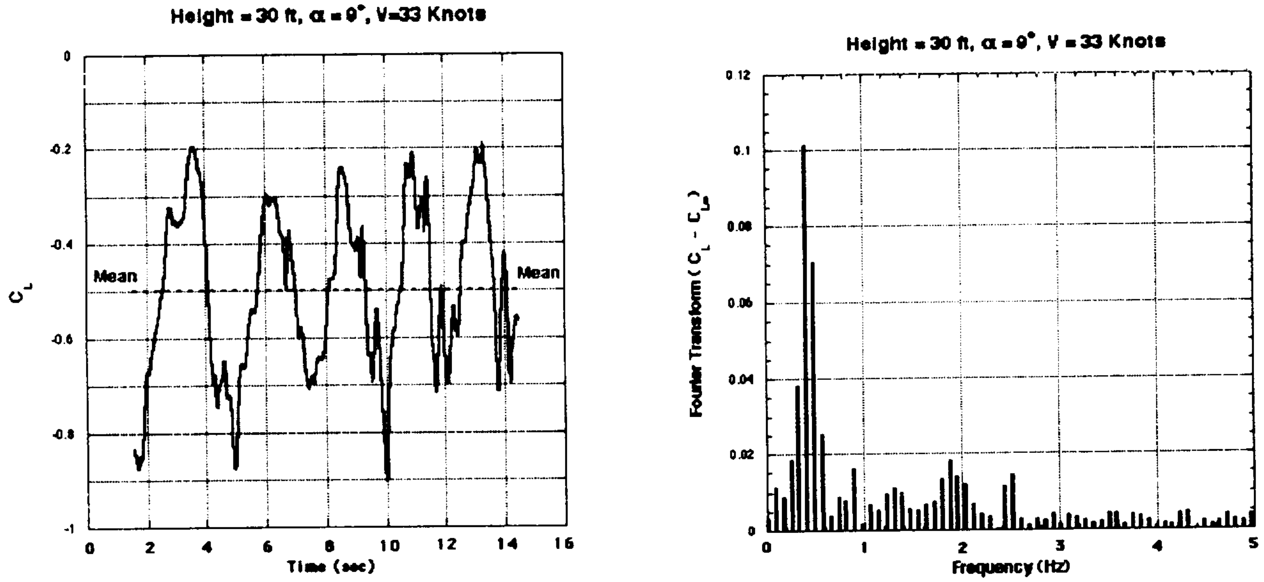

Fig. 6 (a) Time history of lift coefficient; (b) Power spectra of lift coefficient.

Figure 7 shows the mean lift coefficient as a function of height and angle of attack for the entire database. The suckdown effect (loss of lift near the ground) is clearly captured. This loss of lift is the result of the jet ground-plane flow inducing low pressures along the underside of the aircraft. A slight drop in lift from 25 to 30 feet is also apparent. This "ground cushion" effect has been observed in the computations and experiments reported in Ref. 5. At h=10ft, the lift was found to decrease when the angle of attack was increased. The Harrier is so close to the ground that the increased capture area of the freestream flow may be inducing even lower pressures on the underside of the aircraft. (*This will be looked into more carefully and reported in the final paper.*)

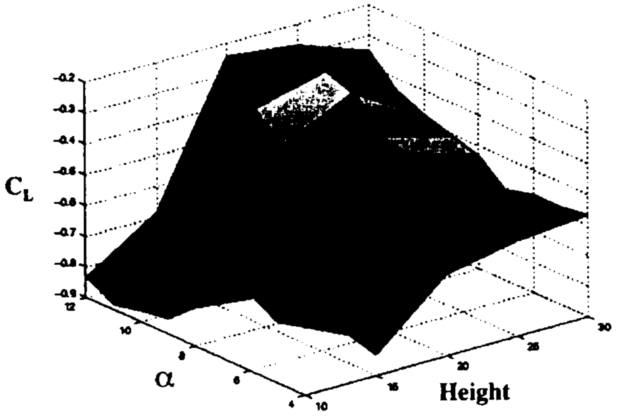

Fig. 7 Mean lift coefficient as a function of height and angle of attack for M=0.05.

A time-dependent streakline animation was carried out for the h=30ft, $\alpha=9^o$ case, in an effort to understand the source of the low frequency oscillation in lift shown in Fig. 6. Solution files were saved every 50 time steps. This corresponds to a physical time step of $\Delta t=3.83$ ms. Two snap-shots from this animation are shown in Fig. 8. The size and position of this vortex change with time, with precisely the same frequency as the lift, f=0.478 Hz. The jet flows themselves also oscillate back and forth with this same frequency, see Fig. 8a and 8b. Thus a direct correlation between the moving ground vortex and jets, and the time-varying lift is established. Cimbala et.al.[2] observed a similar "puffing" behavior of the ground vortex in their jet in crossflow experiment. They concluded that the growth in the vortex size had to do with the ground jets feeding mass into the vortex. When too much fluid accumulated, the vortex would burst, shrink in size, and begin the growing process again. The streakline animation for the Harrier showed the same trend.

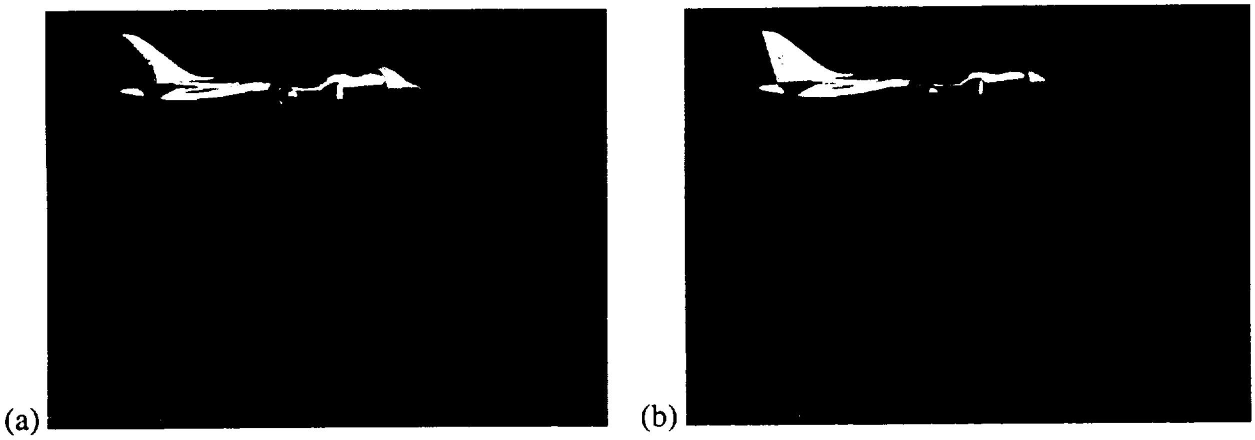
(a) (b)

Fig. 8 Side view of time-dependent streaklines colored by temperature. M=0.05 (33 kts), h=30ft, $\alpha=9^{\circ}$.

A perspective view of the ground vortex is shown in Fig. 9. Streakline particles are now rendered as small spheres rather than pixels to emphasize the ground-vortex structure rather than the jet flow. A secondary ground vortex periodically forms in front of the ground vortex, as in the 10 foot case, see Fig. 5. This secondary vortex is formed once again by the jet fountain, and is drawn upward by the inlet. However, this time the vehicle is sufficiently high so that this secondary flow is not ingested into the inlet. Instead, this secondary flow in entrained into the primary ground vortex, and constitutes a second mass source that contributes to the bursting of the ground vortex.

Fig. 9 Perspective view of time-dependent streaklines colored by temperature. M=0.05 (33 kts), h=30ft, $\alpha=9^{\circ}$.

A snapshot from a streakline animation of the flow over the horizontal tail is shown in Fig. 10. Particles were "seeded" on the underside of the fuselage, near the jet-fountain separation line, and along the horizontal tail surface. For the most part, the jet fountain passes underneath the horizontal tail, resulting in a fairly benign flow. However, occasionally some of the jet fountain will strike the leading edge of the horizontal tail. When this happens, a vertical swirling vortex temporarily forms and ejects fluid in the vertical direction, see Fig. 10. This phenomenon occurs due to the jet fountain interacting with the low-speed ambient flow. Aircraft operating at normal, high-speed flight conditions do not typically experience these low-speed structures. Over 100 MB of data and 1600 solution files were used in these streakline animations.

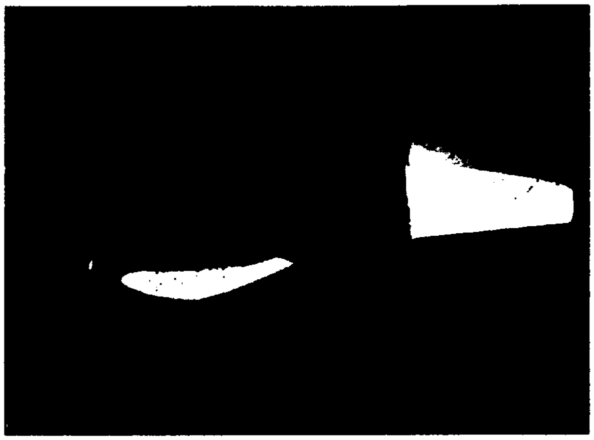

Fig. 10 Time-dependent streaklines on the horizontal tail.
M=0.05 (33 kts), h=30ft, α=9°.

A streakline animation was also carried out for a 10 foot case, with α=9°, and a snapshot from this animation is shown in Fig. 11. Once again, particles are rendered as spheres and colored by temperature. The ground vortex rollup, separation line and core are clearly visible. Once again, a secondary vortex forms in front of the ground vortex. Due to the aircraft's close proximity to the ground, this secondary vortex is ingested into the inlet.

Fig. 11 Perspective view of time-dependent streaklines colored by temperature. M=0.05 (33 kts), h=10ft, α=9°.

The streakline flow structure for the horizontal tail is shown in Fig. 12. A vortex, colored white, comes down and impacts the upper surface of the horizontal tail. The resulting surface flow swirls outward and then up, forming a very stable and persistent toroidal structure. It was difficult to find seed points to clearly highlight the origin of this vortex in the figure. However, experimenting in real time with different seed locations, and tracking the vortex "backward" in time indicated that the vortex begins somewhere near the juncture of the horizontal tail's trailing edge, vertical tail, and fuselage. Additional flow visualization also indicated that the tip vortex shed from the deflected wing flap passes over the horizontal tail, just outboard of this swirling flow. The jet fountain also seems to play a role in pushing some of the ambient flow up over the horizontal tail to form this complex flow structure.

Fig. 12 Time-dependent streaklines on the horizontal tail.
M=0.05 (33 kts), h=10ft, α=9°.

Conclusions

Fortyfive time-accurate Reynolds-averaged Navier-Stokes flow simulations for a Harrier YAV-8B powered-lift aircraft in ground effect have been presented. The freestream Mach number was M=0.05 (33 Kts), and the Reynolds number was 15.2 million based on the fuselage length. The angle of attack range was $4^\circ \leq \alpha \leq 12^\circ$ with a one degree increment, and the height range was $10\text{ft} \leq h \leq 30\text{ft}$ with a 5 foot increment. These flow conditions are typical of those required to establish a static S&C database and aerodynamic model for fight simulation. This paper is a first step towards this goal. Automation played a key role in streamlining and simplifying the grid generation, flow solution, and post-processing processes. Automation also kept the user work load to a manageable level. Numerical time accuracy was established through a series of time-step refinements.

The computed flows were found to by highly unsteady and characterized by very low frequencies, e.g., 0.478 Hz. A direct correlation between vortex puffing, jet-flow movement, and the unsteady aerodynamic lift was established using streakline visualization and an FFT spectral analysis. Similar frequencies and flow structure interactions have been observed experimentally for a round jet in a crossflow. Moreover, this experiment attributes vortex puffing to the continual addition of jet-flow mass to the ground vortex; a process consistent with the computed Harrier streakline visualization. A secondary vortex formed upwind of the ground vortex, due to a jet fountain flow. This vortex was either entrained into the ground vortex at the higher heights, or was ingested by the inlet when the Harrier was closer to the ground. Unsteady vortex structures also occurred on the horizontal tail due to complex interactions between the jet fountain, flap-tip vortex, and the low-speed ambient flow. The computations captured hot gas ingestion, suckdown, and ground cushion effects.

Overall, the present results show promise for computing large numbers of RANS solutions for powered-lift aircraft in ground effect. These computations are possible through the use of large multiprocessor single-image supercomputers and process automation.

The final paper will include:

- A grid-refinement study;
- Comparison of computed jet-flow trajectories with infrared flight-test data;
- Additional post-processing analysis of the h=10ft cases.

References

[1] Siuru, W. D., "British Aerospace and McDonnell Douglas Harrier AV-8A/B," Aero Publishers, INC., Fallbrook, California, 1985.

[2] Cimbala, J. M., Billet, M. L., Gaublomme, D. P., and Ofelein, J. C., "Experiments on the Unsteadiness Associated with a Ground Vortex," *AIAA Journal of Aircraft*, Vol. 28, No. 4, April 1991, pp. 261-267.

[3] Van Dalsem, W. R., Panaras, A. G., and Steger, J. L., "Numerical Investigation of a Jet in Ground Effect with a Crossflow," SAE Paper 872344, December 1987.

[4] Baldwin, B. S., and Lomax, H., "Thin Layer Approximation and Algebraic Model for Separated Turbulent Flow," AIAA Paper 78-257, 1978.

[5] Van Dalsem, W. R., Chawla, K., Smith, M. H., and Abeloff, P. A., "Numerical Simulation of Powered-Lift Flows," International Powered Lift Conference Proceedings, The Royal Aeronautical Society, August 1990, pp. III.16.1-14.

[6] Barata, J., Durao, D., and McGuirk, J., "Numerical Study of Single Impinging Jets Through a Crossflow," AIAA Paper 89-0449, January 1989.

[7] Barata, J., "Numerical and Experimental Study of Fountain Flows Produced by Multijet Impingement on a Ground Plane," AIAA Paper 91-1806, June 1991.

[8] Jones, W. P., Launder, B. E., "The Calculation of Low-Reynolds-Number Phenomena with a Two-Equation Model of Turbulence," *International Journal of Heat and Mass Transfer*, Vol. 16, June 1973, pp. 1119-1130.

[9] Chawla, K., and Van Dalsem, W. R., "Numerical Simulation of a Powered-Lift Landing," AGARD-CP-534, April 1993, pp.32-1-32-10.

[10] Roth, K. R., "Comparison of Computation with Experiment for a Geometrically Simplified Powered-Lift Model," *AIAA Journal of Aircraft*, Vol. 34, No. 2, March-April 1997, pp. 160-167.

[11] Degani, D. and Schiff, L. B., "Computation of Supersonic Viscous flows Around Pointed Bodies at Large Incidence," AIAA Paper 83-0034, January 1983.

[12] Gea, L. M., Chyu, W. J., Stortz, M. W., Roberts, A. C., and Chow, C. Y., "Flight Test and Numerical Simulation of Transonic Flow Around YAV-8B Harrier II Wing," AIAA Paper 91-1628, June 1991.

[13] Mysko, S. J., Chyu, W. J., Stortz, M. W., and Chow, C. Y., "Navier-Stokes Simulation of External/Internal Transonic Flow on the Forebody/Inlet of the AV-8B Harrier II," AIAA Paper 93-3057, July 1993.

[14] Smith, M. H., Chawla, K., and Van Dalsem, W. R., "Numerical Simulation of a Complete STOVL Aircraft in Ground Effect," AIAA 91-3293-CP, September 1991.

[15]Buning, P. G., Jespersn, D. C., Pulliam, T. H. Chan, W. M. Slotnick, J. P., Krist, S. E., and Renze, K. J., "OVERFLOW User's Manual," NASA.

[16]Rogers, S. E., Roth, K., Nash, S. M., Baker, M. D., Slotnick, J. P., Whitlock, M., and Cao, H. V., "Advances in Overset CFD Processes Applied to Subsonic High-Lift Aircraft," AIAA Paper 2000-4216, August 2000.

[17]Suhs, N. E., and Tramel, R. W., "PEGSUS 4.0 User's Manual," AEDC-TR-91-8, November 1991, Arnold Engineering Development Center, Arnold AFB, TN.

[18]Murman, S. M., Chaderjian, N. M., Pandya, S., "Automation of a Numerical S&C Database Generation for the Harrier in Ground Effect," Submitted for presentation to the 40th AIAA Aerospace Sciences Meeting & Exhibit, Reno, Nevada, January 2002.

[19]Pulliam, T. H., and Chaussee, D. S., "A Diagonal Form of an Implicit Approximate-Factorization Algorithm," *Journal of Computational Physics*, Vol. 39, No. 2, 1981, pp. 347-363.

[20]Taft, J. R., "Multi-Level Parallelism, "A Simple Highly Scalable Approach to Parallelism for CFD," HPCCP/CAS Workshop Proceedings, (C. Schulbach, ed.), 1998.

[21]Spalart, P. R., Allmaras, S. R., "A One-Equation Turbulence Model for Aerodynamic Flows," AIAA Paper 92-0439, January 1992.